Acta Cryst. (1999). B**55**, 683–697

Total neutron diffraction: a route to the correct local structure of disordered $LaMo_2O_5$ and its application to the model compound $Zn_2Mo_3O_8$

Simon J. Hibble,[a]* Steven P. Cooper,[a] Saban Patat[a] and Alex. C. Hannon[b]

[a]*Department of Chemistry, University of Reading, Whiteknights, PO Box 224, Reading RG6 6AD, England, and* [b]*ISIS Facility, Rutherford Appleton Laboratory, Chilton, Didcot, Oxon OX11 0QX, England. E-mail: s.j.hibble@rdg.ac.uk*

(*Received 2 October 1998; accepted 8 March 1999*)

Abstract

Analysis of Bragg diffraction is the normal route to the structure of crystalline materials. Here we demonstrate the use of total neutron diffraction in determining the local structure in the disordered lanthanum molybdate $LaMo_2O_5$. An average structure with space-group symmetry $P6_3/mmc$ accounts for the Bragg scattering and shows that the compound contains the rare Mo_6O_{18} cluster and a unique type of Mo—Mo bonded sheet. However, this gives an incomplete picture of the structure, since it does not reveal how the sites with fractional occupancy are occupied at a local level. Two models describing possible local structures are constructed by removing symmetry elements present in the average structure. Total correlation functions, $T(r)$, calculated from these structures, with space-group symmetry $P6_3mc$ and $P\bar{3}m1$, are compared with the experimental $T(r)$ to show the validity of these local structures. The close relationship between the $T(r)$'s of the component structures gives an insight into why disorder occurs in $LaMo_2O_5$. The calculated and experimental $T(r)$'s for a model compound, $Zn_2Mo_3O_8$, are compared to show the agreement expected from an ordered crystalline material. Remaining discrepancies between our model and the experimental $T(r)$ give an insight into the origin of additional disorder in $LaMo_2O_5$.

1. Introduction

Disorder is a universal problem in the determination and description of the structure of solids. Thermal disorder, for example, is always present, and a large number of models of differing complexity have been developed. Static disorder can range from the small number of defects expected in a crystalline material not at absolute zero to the total lack of long-range order characteristic of amorphous materials. The goal in the structural study of amorphous materials is to determine local structure. This is also the aim of the chemical crystallographer, but in this case the techniques normally employed yield an average structure in which positional and occupational disorder can sometimes lead to an incorrect local structural picture.

The techniques used for determining the structure of amorphous materials can be usefully applied to disordered crystalline materials. Fourier transformation of the interference function rather than merely of the Bragg intensities yields the differential correlation function, $D(r)$, and after addition of the average scattering density the total correlation function, $T(r)$. These functions give information on interatomic distances directly, without the need for a crystalline model. Applications of this method include the direct determination of C—C bond lengths in C_{60} (Soper *et al.*, 1992), the direct determination of the Si—O bond length in β-cristobalite (Dove *et al.*, 1997), determination of the local structure in ferroelectrics (Teslic *et al.*, 1997) and the determination of Mn—O bond lengths in the giant magnetoresistance manganates $La_{1-x}Sr_xMnO_3$ (Louca *et al.*, 1997).

Ideally, both the Bragg scattering and diffuse scattering would be modelled. We have attempted to do this in our studies of the lithium molybdates Li_2MoO_3 and $Li_4Mo_3O_8$ (Hibble *et al.*, 1997*a*), and $LiMoO_2$ (Hibble *et al.*, 1997*b*). In these studies we used the Bragg scattering to determine the average structure and the total neutron scattering to determine local structure. Modelling of the correlation function, $T(r)$, gave structural information on the metal–metal bonded clusters present in these reduced molybdates, which were not revealed by only modelling the Bragg scattering.

We recently determined the average structure of $LaMo_2O_5$ using Bragg diffraction at 300 K on the time-of-flight neutron diffractometer POLARIS at the Rutherford Appleton Laboratory (Hibble *et al.*, 1998). This showed that the compound contains the rare Mo_6O_{18} cluster and a unique type of Mo—Mo bonded sheet (Fig. 1). However, in the model accounting for the Bragg scattering in space group $P6_3/mmc$, two-thirds of the atom sites have 50% occupancy. Fig. 2 shows a projection of the average structure. It was obvious that certain atoms would never occur as near neighbours in the local structure; for example, there are pairs of O atoms between the molybdenum sheets that are separated by less than 0.6 Å. Only one site from each of the

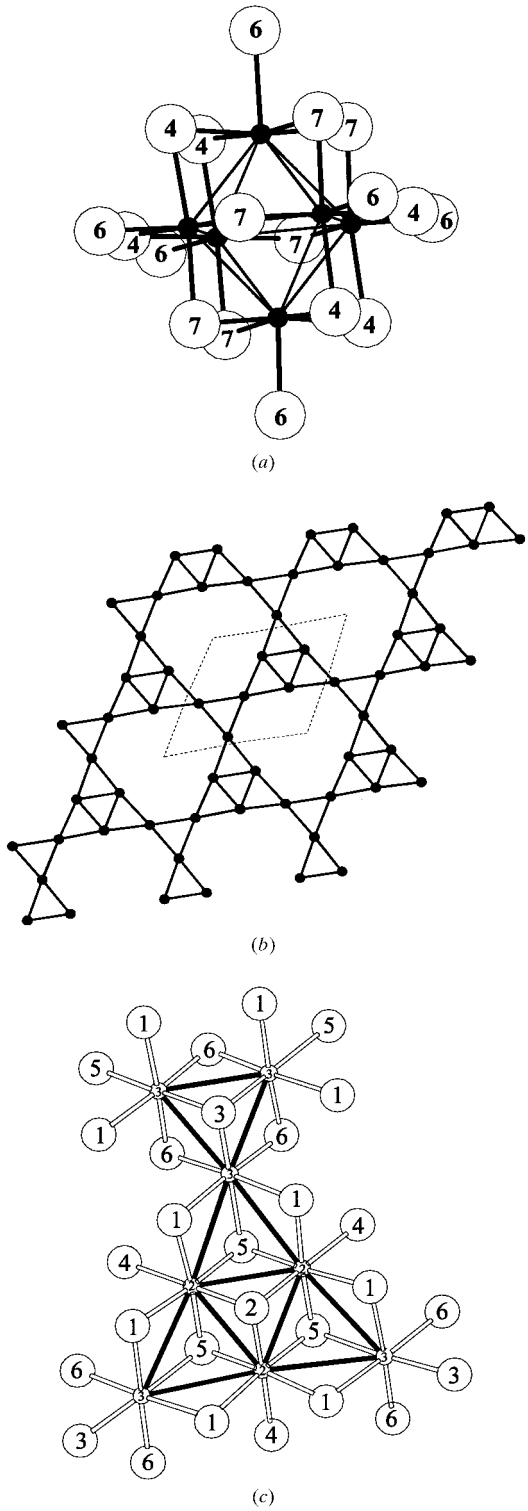

Fig. 1. (*a*) The Mo_6O_{18} unit (solid circles: Mo1; large circles: O). Atom labels correspond to structure A (Table 3). (*b*) An extended view of the infinite Mo—Mo bonded sheets present in $LaMo_2O_5$. (*c*) A section of the infinite Mo—Mo bonded sheet present in $LaMo_2O_5$ with attached O atoms (small circles: Mo; large circles: O). Atom labels correspond to structure A (Table 3).

pairs can be occupied. Closer inspection reveals that adjacent molybdenum sheets cannot both be occupied. This would produce too many short Mo—Mo bonds in the range 2.5–2.8 Å and unreasonable coordination spheres around the O atoms between the sheets. Using chemical and physical reasoning, it was possible to account for the average structure in terms of local structures. In this paper we use total neutron scattering data, which contain information on both long-range and short-range structure, to prove the validity of the picture we presented previously and to produce detailed models of the component structures. The total neutron scattering intensities were measured at 13 K to minimize the effect of thermal disorder, and as a first step we refined our average structural model obtained from room-temperature data. As a guide to the quality of the final agreement between our theoretical and experimentally determined $T(r)$'s we have carried out similar calculations for the ordered model compound $Zn_2Mo_3O_8$ (Ansell & Katz, 1966).

2. Theory

The basic quantity measured in neutron diffraction is the differential cross section (Hannon *et al.*, 1990)

$$\mathrm{d}\sigma/\mathrm{d}\Omega = I(Q) = I^s(Q) + i(Q), \tag{1}$$

where $I^s(Q)$ is known as the self-scattering and $i(Q)$ is known as the distinct scattering. Q is the magnitude of the scattering vector (momentum transfer) for elastic scattering, given by

$$Q = (4\pi \sin\theta)/\lambda. \tag{2}$$

After subtracting the self-scattering, the distinct scattering is Fourier transformed to give the differential correlation function $D(r)$

$$D(r) = (2/\pi) \int_0^{Q_{\max}} Qi(Q)M(Q)\sin(rQ)\,\mathrm{d}Q, \tag{3}$$

where $M(Q)$ is a modification function (used to take into account that the diffraction pattern is measured up to a finite momentum transfer $Q_{\max}$ and not to infinity). This is converted to the total correlation function $T(r)$

$$T(r) = D(r) + T^0(r) \tag{4}$$

$$T^0(r) = 4\pi r g^0 \left(\sum_l c_l \bar{b}_l\right)^2. \tag{5}$$

g^0 (= N/V) is the macroscopic number density of scattering units, c_l is the atomic fraction and $\bar{b}_l$ is the coherent neutron scattering length for element l. The modification function is a step function cutting off at $Q = Q_{\max}$ and the one used is that due to Lorch (1969)

Table 1. *Atomic parameters for $Zn_2Mo_3O_8$ from the Rietveld refinement*

	Multiplicity	*x*	*y*	*z*	*U* (Å^2)
Zn1	2	1/3	2/3	0.5155 (4)	0.0039 (5)
Zn2	2	1/3	2/3	0.9491 (6)	0.0039 (5)
Mo1	6	0.1475 (2)	0.8525 (2)	1/4	0.0032 (5)
O1	2	0	0	0.8921 (5)	0.0044 (3)
O2	2	1/3	2/3	0.1450 (5)	0.0044 (3)
O3	6	0.4881 (3)	0.5119 (3)	0.3658 (3)	0.0044 (3)
O4	6	0.1662 (3)	0.8338 (3)	0.6334 (4)	0.0044 (3)

Space group $P6_3mc$, $a = b = 5.77322\,(1)$, $c = 9.91231\,(4)$ Å, number of reflections used in the refinement = 309, $R_{wp} = [\sum_i w_i|Y_i(\text{obs}) - Y_i(\text{calc})|^2 / \sum_i w_i Y_i(\text{obs})^2]^{1/2} = 0.047$, where R_{wp} is the weighted profile *R* factor, w_i is the weight for point *i*, Y_i is the intensity of point *i*. Derived $\sigma_{ll'}$'s for the partial correlation functions, and agreement factors $R_{T(r)}$ and $R_{D(r)}$ for the $Zn_2Mo_3O_8$ Rietveld refinement are: $\sigma_{O-O} = 0.095$, $\sigma_{Mo-O} = 0.087$, $\sigma_{Mo-Mo} = 0.080$, $\sigma_{Zn-Zn} = 0.088$, $\sigma_{Zn-O} = 0.092$, $\sigma_{Zn-Mo} = 0.084$ Å, $R_{T(r)}$(1.5–3.3 Å) = 0.101, $R_{T(r)}$(1.5–13.7 Å) = 0.048, $R_{D(r)}$(1.5–3.3 Å) = 0.156, $R_{D(r)}$ = (1.5–13.7 Å) = 0.206.

$$M(Q) = \sin(Q\Delta r)/Q\Delta r \quad \text{for} \quad Q < Q_{max} \tag{6}$$

$$= 0 \quad \text{for} \quad Q > Q_{max}, \tag{7}$$

where $\Delta r = \pi/Q_{max}$. Use of this modification function eliminates termination ripples from $T(r)$.

To calculate $T(r)$ for our models we employed the program *XTAL* (Hannon, 1993) and the *GENIE* (David *et al.*, 1986) input program *RDF* (Hannon, 1993). *XTAL* produced the partial pair distribution functions $g_{ll'}$ from the atomic and lattice parameters of our model.

$$g_{ll'}(r) = \left(1/\sum_{i=1}^{N_l} w_i\right) \sum_{j=1}^{N_l} \sum_{j' \neq j=1}^{N_{l'}} w_j w_{j'} \langle \delta(\mathbf{r} + \mathbf{R}_j - \mathbf{R}_{j'}) \rangle, \tag{8}$$

where $\mathbf{R}_j$ is the position of the *j*th atom and w_i is the occupancy of the *i*th atom. The *j*, *j'* sums are over the N_l, $N_{l'}$ atoms of element *l*, *l'* and $j' \neq j$ means that *j* and *j'* are not allowed to refer to the same atom. $g_{ll'}$ may be interpreted as the number density of atoms of element *l'* at a distance *r* (= $|\mathbf{r}|$) from an origin atom of element *l*, averaged over all possible origin atoms and directions of **r**. The weighted partial correlation functions $t_{ll'}$

$$t_{ll'}(r) = 4\pi r g_{ll'}(r) \tag{9}$$

were then summed to yield the total correlation function $T(r)$

$$T(r) = \sum_{ll'} c_l \bar{b}_l \bar{b}_{l'} t_{ll'}(r), \tag{10}$$

where c_l (= N_l/N) is the atomic fraction for element *l* and the *l* and *l'* summations are both over the elements of the sample. The functions $t_{ll'}(r)$ were broadened using a Gaussian function to simulate the broadening of experimental data owing to thermal motion. This function

$$P(r) = 1/[\sigma(2\pi)^{1/2}] \exp[(r - r_0)^2)/2\sigma^2] \tag{11}$$

preserved coordination numbers.

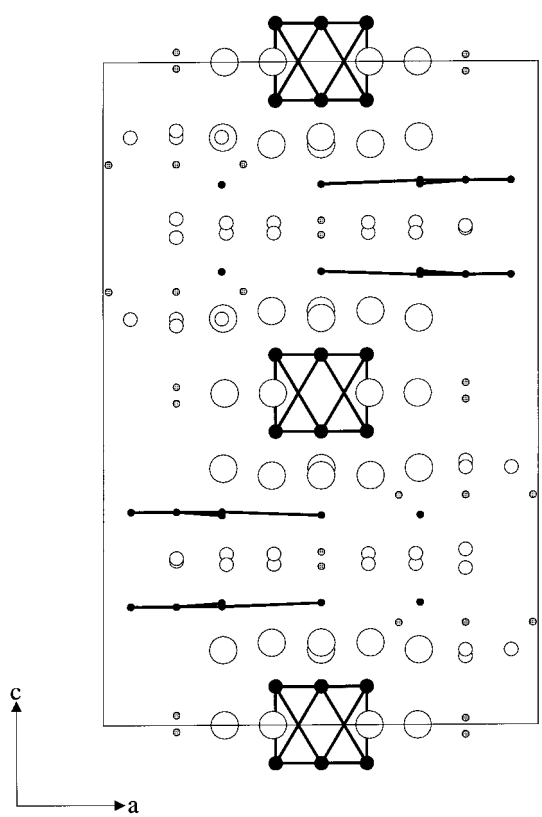

Fig. 2. The average unit cell for $LaMo_2O_5$ viewed along the [120] direction (space group $P6_3/mmc$; solid circles: Mo; open circles: O; spotted circles: La; small and large circles represent atom sites with occupancies of 0.5 and 1, respectively). Only Mo—Mo bonds are shown. Light lines indicate the unit cell.

3. Experimental

3.1. *Sample preparation*

3.1.1. *Lanthanum molybdate*. $LaMo_2O_5$ was prepared by heating a mixture of Mo powder (Aldrich), MoO_2 and La_2O_3 (Aldrich) in the required stoichiometric quantities at 1498 K for 72 h in an alumina tube contained inside a sealed evacuated silica ampoule. The

Table 2. *Atomic parameters for $LaMo_2O_5$ from the Rietveld refinement of the average structure*

	Multiplicity	*x*	*y*	*z*	*U* (Å^2)	Occupancy
La1	12	0.5112 (8)	0.4888 (8)	0.8438 (8)	0.010 (2)	0.5†
La2	2	0	0	0.260 (1)	0.010 (2)	0.5†
La3	4	1/3	2/3	0.984 (1)	0.010 (2)	0.5†
La4	4	1/3	2/3	0.012 (1)	0.010 (2)	0.5†
Mo1	12	0.1066 (6)	0.8934 (6)	0.9428 (3)	0.008 (1)	1.0
Mo2	12	0.769 (1)	0.231 (1)	0.6868 (8)	0.008 (1)	0.5†
Mo3	12	0.561 (1)	0.439 (1)	0.1784 (7)	0.008 (1)	0.5†
O1	24	0.330 (1)	0.000 (1)	0.242 (7)	0.0044 (9)	0.5†
O2	4	1/3	2/3	0.2617 (7)	0.0044 (9)	0.5†
O3	4	1/3	2/3	0.752 (1)	0.0044 (9)	0.5†
O4	12	0.1138 (6)	0.2276 (7)	0.1234 (3)	0.0044 (9)	1.0
O5	12	0.560 (2)	0.120 (3)	0.6157 (9)	0.0044 (9)	0.5†
O6	12	0.454 (1)	0.2268 (7)	0.1130 (5)	0.0044 (9)	1.0
O7	12	0	0.334 (1)	0	0.0044 (9)	1.0
O10	4	1/3	2/3	0.399 (1)	0.0044 (9)	0.5†

† The occupancy must be 0.5 in order to avoid physically unreasonable contacts in the local structure. Space group $P6_3/mmc$, $a = b = 8.3680$ (7), $c = 19.13687$ (4) Å, number of reflections used in the refinement = 312, $R_{wp} = 0.048$. Derived $\sigma_{ll'}$'s for the partial correlation functions (from the Rietveld refinement of $Zn_2Mo_3O_8$), and agreement factors $R_{T(r)}$ and $R_{D(r)}$ are: $\sigma_{O-O} = 0.095$, $\sigma_{Mo-O} = 0.087$, $\sigma_{Mo-Mo} = 0.080$, $\sigma_{La-La} = 0.088$ Å, $\sigma_{La-O} = 0.092$, $\sigma_{La-Mo} = 0.084$ Å, $R_{T(r)}$(1.5–3.3 Å) = 0.320, $R_{T(r)}$(1.5–13.7 Å) = 0.124, $R_{D(r)}$(1.5–3.3 Å) = 0.545, $R_{D(r)}$(1.5–13.7 Å) = 0.633.

MoO_2 precursor was synthesized from Mo powder (Aldrich) and MoO_3 (Aldrich) heated together at 773 K for 24 h followed by a further 24 h at 1273 K in a sealed evacuated silica ampoule.

3.1.2. *Zinc molybdate*. $Zn_2Mo_3O_8$ was prepared by grinding together stoichiometric quantities of ZnO (Aldrich), MoO_3 (Aldrich) and Mo (Aldrich), sealing the reaction mixture in an evacuated silica tube and heating at 773 K for 24 h and 1173 K for 48 h. The mixture was reground and reheated at 1173 K for 48 h in an evacuated sealed silica tube.

3.2. *Data collection*

Time-of-flight powder neutron diffraction intensities were measured on the LAD diffractometer at ISIS, Rutherford Appleton Laboratory, Chilton, Didcot, England (Howells, 1980). LAD is equipped with pairs of detector banks at 5, 10, 20, 35, 58, 90 and 150°. Powdered samples, 6.801 g of $LaMo_2O_5$ and 6.264 g of $Zn_2Mo_3O_8$, were loaded into cylindrical vanadium sample holders of nominal diameter 8 mm. The effective density of each sample, as used in the data-correction routines, was determined from the sample depth. The samples were cooled to 12–13 K using a closed-cycle refrigerator. Data were collected over the time-of-flight range 100–19750 μs, and analysed using the Q range 0.25–50 Å^{-1} and extrapolating to $Q = 0$ Å^{-1}. Background runs were collected on the empty can and empty spectrometer, and data were collected for a standard vanadium rod.†

† Supplementary data for this paper are available from the IUCr electronic archives (Reference: BR0083). Services for accessing these data are described at the back of the journal.

4. Data reduction and analysis

4.1. *Rietveld analysis*

Data for Rietveld analysis were obtained by combining the signals from the two 150° detector banks and normalizing to the neutron flux. Rietveld refinements for $LaMo_2O_5$ and $Zn_2Mo_3O_8$ were carried out using the program *TF12LS* (David *et al.*, 1992) over the *d*-space ranges 0.9699–3.5490 and 0.7845–3.6424 Å, respectively, with the peak shape modelled by a pseudo-Voigt function convoluted with a double exponential function. The coherent scattering lengths used for La, Mo, Zn and O were 0.8240, 0.6715, 0.5680 and 0.5803 × 10^{-14} m, respectively (Koester & Yelon, 1982). As a starting point for our refinement of the structure of $LaMo_2O_5$ we used the atomic parameters we had previously obtained in our room-temperature study (Hibble *et al.*, 1998). In our refinement of the $Zn_2Mo_3O_8$ structure we commenced the refinement using the atomic parameters determined previously by Ansell & Katz (1966). The scale and five polynomial background parameters were refined first, followed by the unit cell, the atomic parameters, independent temperature factors for each atom type and finally the peak-shape parameters. The refined lattice and atomic parameters are given in Tables 1 and 2, and I_{obs}, I_{calc} and the difference plots, $(I_{obs} - I_{calc})$/s.u., are shown in Figs. 3(*a*) and 3(*b*). The atomic parameters for $LaMo_2O_5$ are in good agreement with those we obtained in the room-temperature study (Hibble *et al.*, 1998) and those for $Zn_2Mo_3O_8$ are in good agreement with those obtained previously by Ansell & Katz (1966). The weak Bragg peaks seen in Fig. 3(*b*) that are not accounted for by our model of $LaMo_2O_5$ (*e.g.* at $d = 2.18$ and 2.83 Å) arise

from $LaMo_2O_5$ and not from impurities. The origin of these peaks, which are broader than those we have modelled, is discussed later. They are also seen in the data we collected at 300 K.

4.2. *Total neutron scattering*

Data for total neutron scattering were obtained by merging the data from all 14 detector banks (over the Q

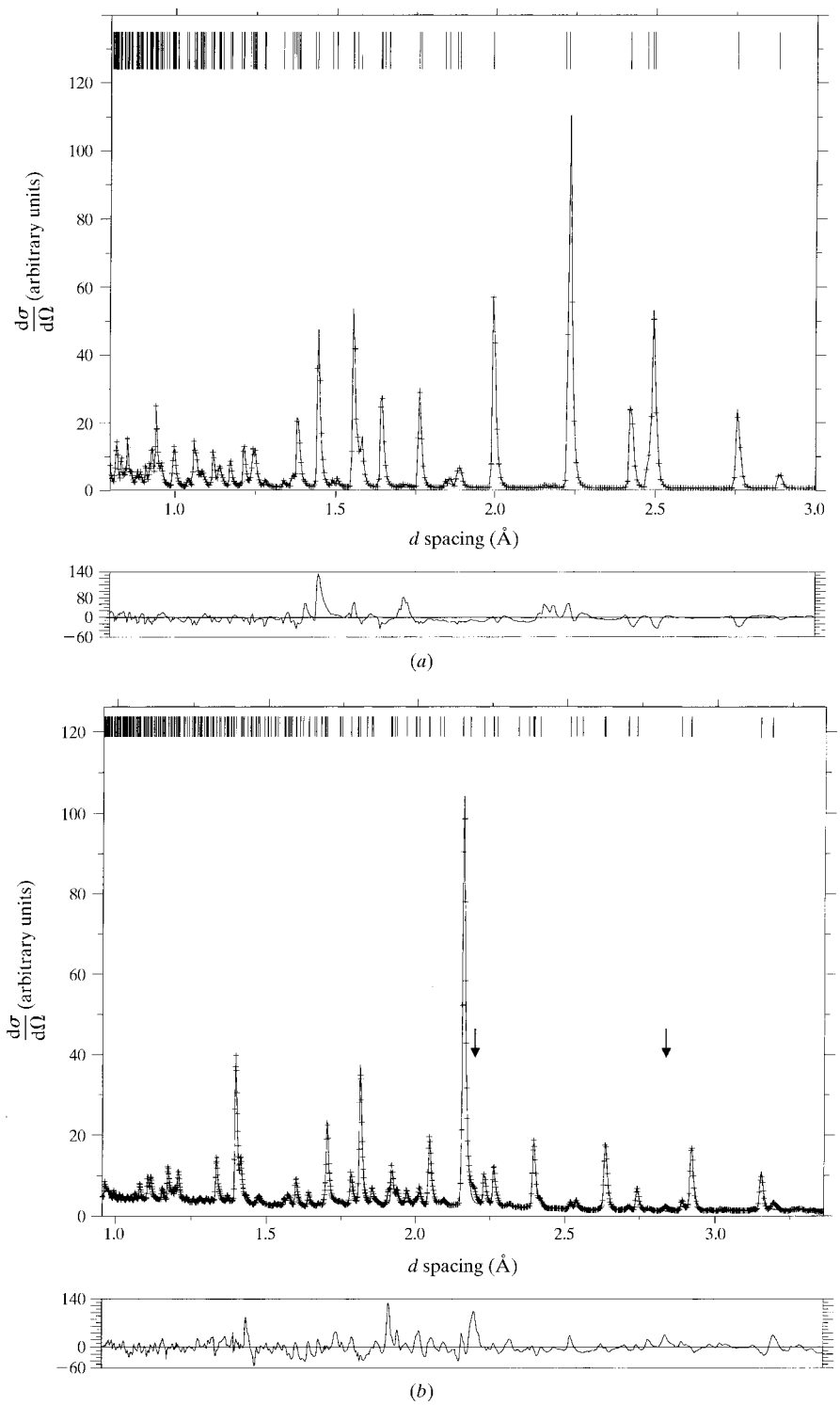

Fig. 3. (*a*) Final fitted profiles [points: observed; line: calculated; lower plot: $(I_{obs} - I_{calc})$/s.u.] from the Rietveld refinement of $Zn_2Mo_3O_8$. Tick lines directly above the diffraction pattern indicate the positions of the allowed reflections. (*b*) Final fitted profiles [points: observed; line: calculated; lower plot: $(I_{obs} - I_{calc})$/s.u.] from Rietveld refinement of $LaMo_2O_5$ using the disordered model in space group $P6_3/mmc$. The arrows indicate the positions of two Bragg peaks unaccounted for by our models.

range 0–50 Å^{-1}) normalized to absolute scattering units, after correcting for detector deadtime, multiple scattering, inelasticity and attenuation using the *ATLAS* suite of programs (Soper *et al.*, 1989).

The interference functions $Qi(Q)$ for $Zn_2Mo_3O_8$ and $LaMo_2O_5$ out to Q = 50 Å^{-1} are shown in Figs. 4 and 5, respectively.

5. Modelling

5.1. *$Zn_2Mo_3O_8$*

The total correlation function, $T(r)_{\rm exp}$, from 0–14 Å obtained by Fourier transforming $Qi(Q)$ according to equation (3) for $Zn_2Mo_3O_8$ is shown in Fig. 6 along with that calculated using the atomic and structural parameters given in Table 1. Thermal broadening was introduced by calculating $\sigma_{ll'}$ values for the partial correlation functions from the thermal parameter assuming

$$\sigma_l^2 = U \tag{12}$$

and using the relationship

$$\sigma_{ll'}^2 = \sigma_l^2 + \sigma_{l'}^2. \tag{13}$$

The agreement between $T(r)_{\rm calc}$ for our models and $T(r)_{\rm exp}$ derived from the experimental data is measured using the R factor

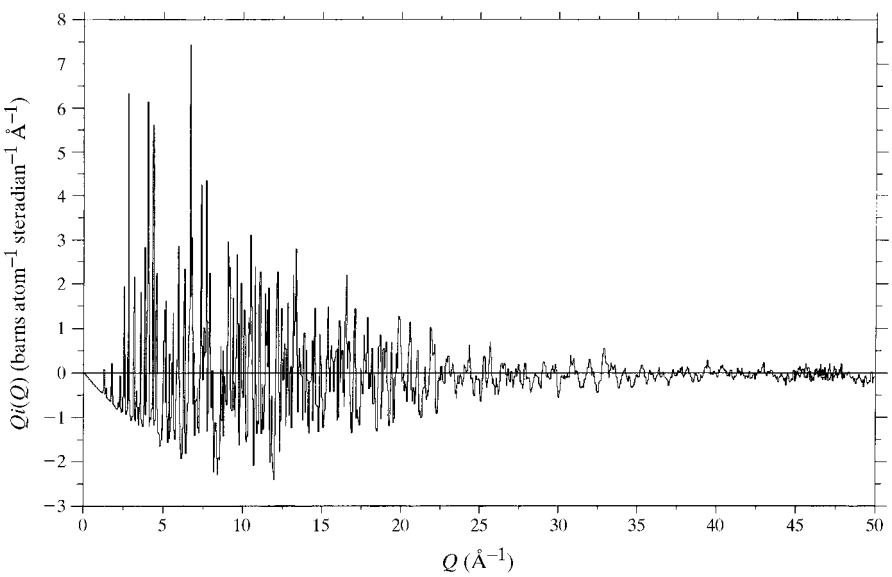

Fig. 4. The interference function $Qi(Q)$ for $Zn_2Mo_3O_8$.

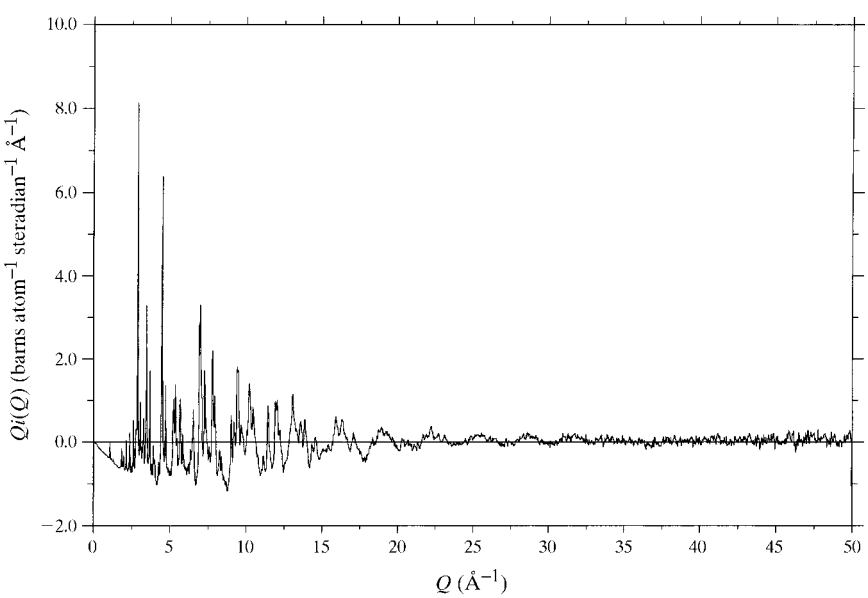

Fig. 5. The interference function $Qi(Q)$ for $LaMo_2O_5$.

$$R_{T(r)} = \left[\sum_i \left|Y_i(\text{obs}) - Y_i(\text{calc})\right|^2 / \sum_i Y_i(\text{obs})^2\right]^{1/2}. \quad (14)$$

This R factor includes a measure of how accurately the effective number density has been determined. It is calculated to a maximum r of 13.7 Å to avoid edge effects in our modelling. The R factor $R_{D(r)}$, which is used by Toby & Egami in their paper on the statistics of correlation functions (Toby & Egami, 1992), is calculated in a similar way and is given in the tables for the different models. In that paper they calculated $D(r)$ without the use of a modification function. We have chosen to employ a modification function, because for our model compound, $Zn_2Mo_3O_8$, termination ripples are significant in the Fourier transform of $Qi(Q)$ even when Q_{max} = 50 Å^{-1}. In the case of the ordered compound $Zn_2Mo_3O_8$ we have a good structural model, and thus the $R_{T(r)}$ factors of 0.101 over the r range 1.5–3.3 Å and 0.048 over the r range 1.5–13.7 Å give a measure of the agreement between $T(r)_{calc}$ and $T(r)_{exp}$ that we should aim to obtain when modelling the local- and medium-range structure in disordered compounds.

5.2. *$LaMo_2O_5$*

The total correlation function $T(r)_{exp}$ from 0–14 Å obtained by Fourier transforming $Qi(Q)$ according to equation (3) for $LaMo_2O_5$ is shown in Fig. 7 with that calculated using the average structure given in Table 2 and estimates of $\sigma_{ll'}$ obtained using the values for $Zn_2Mo_3O_8$ and assuming that $U_{La} = U_{Zn}$. These values were used since the U values obtained for $LaMo_2O_5$, a disordered material, will contain both a thermal and a static contribution. The agreement is poor [$R_{T(r)}$(1.5–3.3 Å) = 0.320 and $R_{T(r)}$(1.5–13.7 Å) = 0.124], showing that the average structure gives an inadequate representation of the true local structure. This is not unexpected, since we know that the two adjacent layers of molybdenum sheets shown in Fig. 2 would not be occupied at the same time. In our previous paper on the structure of $LaMo_2O_5$ (Hibble *et al.*, 1998), we used bond-length–bond-order and close contact considera-

Table 3. *Atomic parameters for structure A (space group $P6_3mc$) used to model T(r)*

	Multiplicity	x	y	z
La1	6	0.5112	0.4888	0.8438
La2	2	0	0	0.2400
La3	2	1/3	2/3	0.9840
La4	2	1/3	2/3	0.5120
Mo1	6	0.1066	0.8934	0.9428
Mo2	6	0.7690	0.2310	0.6868
Mo3	6	0.5610	0.4390	0.1780
Mo4	6	0.8934	0.1066	0.0572
O1	12	0.3300	0.0000	0.2420
O2	2	1/3	2/3	0.2650
O3	2	2/3	1/3	0.2520
O4	6	0.11380	0.2276	0.1234
O5	6	0.4400	0.8800	0.1157
O6	6	0.4536	0.2268	0.1130
O7	12	0.0000	0.3339	0.0000
O8	6	0.5464	0.77532	0.8870
O9	6	0.8862	0.7724	0.8770
O10	2	1/3	2/3	0.3990

Derived $\sigma_{ll'}$'s for the partial correlation functions, and agreement factors $R_{T(r)}$ and $R_{D(r)}$ for the three modelling regimes are: (i) from the Rietveld refinement for $LaMo_2O_5$ σ_{O-O} = 0.060, σ_{Mo-O} = 0.070, σ_{Mo-Mo} = 0.070, σ_{La-La} = 0.147, σ_{La-O} = 0.114, σ_{La-Mo} = 0.115 Å, $R_{T(r)}$(1.5–3.3 Å) = 0.190, $R_{T(r)}$(1.5–13.7 Å) = 0.125, $R_{D(r)}$(1.5–3.3 Å) = 0.326, $R_{D(r)}$(1.5–13.7 Å) = 0.636; (ii) from the $Zn_2Mo_3O_8$ Rietveld refinement σ_{O-O} = 0.095, σ_{Mo-O} = 0.087, σ_{Mo-Mo} = 0.080, σ_{La-La} = 0.088, σ_{La-O} = 0.092, σ_{La-Mo} = 0.084 Å, $R_{T(r)}$(1.5–3.3 Å) = 0.194, $R_{T(r)}$(1.5–13.7 Å) = 0.091, $R_{D(r)}$(1.5–3.3 Å) = 0.331, $R_{D(r)}$(1.5–13.7 Å) = 0.467; (iii) from the $Zn_2Mo_3O_8$ Rietveld refinement with σ_{O-O} fixed at 0.15 Å σ_{O-O} = 0.150, σ_{Mo-O} = 0.087, σ_{Mo-Mo} = 0.080, σ_{La-La} = 0.088, σ_{La-O} = 0.092, σ_{La-Mo} = 0.084 Å, $R_{T(r)}$(1.5–3.3 Å) = 0.108, $R_{T(r)}$(1.5–13.7 Å) = 0.063, $R_{D(r)}$(1.5–3.3 Å) = 0.184, $R_{D(r)}$(1.5–13.7 Å) = 0.320.

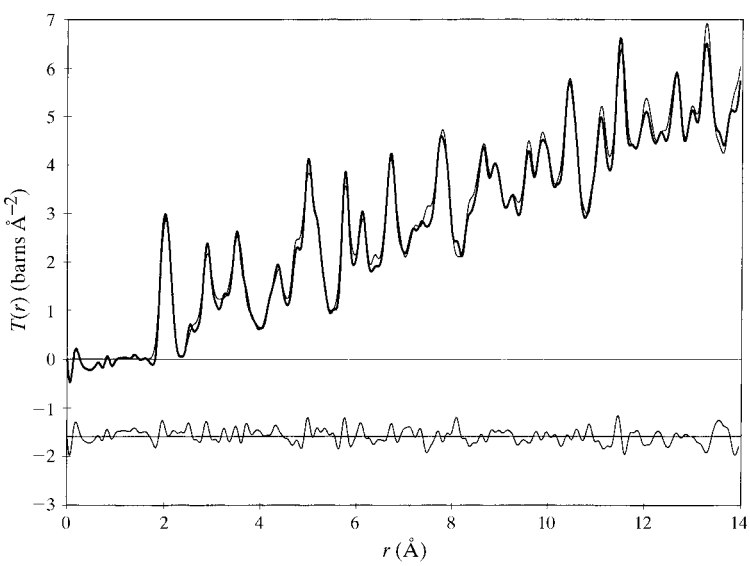

Fig. 6. $T(r)_{exp}$ (heavy line) and $T(r)$ calculated from the parameters obtained from Rietveld refinement of $Zn_2Mo_3O_8$ (light line). The difference is shown below.

tions to devise a plausible description of the local structure of $LaMo_2O_5$. Here we adopt a different approach, using consideration of local symmetry to extract local structures from the average structure. These structural models have the benefit of providing an easy visualization of the different possibilities for local structures and a route to futher investigations on electronic structure, because they have crystallographic symmetry. Most importantly, $T(r)$ can be calculated from such structures and compared with the experimentally determined correlation function $T(r)_{exp}$.

We found that we could construct two chemically plausible models in non-isomorphic subgroups of the space group $P6_3/mmc$ used to describe the average structure of $LaMo_2O_5$:

Structure A. Removing a centre of symmetry from space group $P6_3/mmc$ produces the maximal non-isomorphic subgroup $P6_3mc$. Choosing an appropriate set of atoms from the average structure yields structure A, shown in projection in Fig. 8. The atomic parameters for structure A are given in Table 3 and the bond lengths are given in Table 4. This structure retains the structural units seen in the average structure, but is ordered with no partially occupied sites.

Structure B. It is also possible to retain the centre of symmetry and construct a model in the maximal non-isomorphic subgroup $P\bar{3}m1$. Again an appropriate set of atoms were chosen from the average structure to yield another possible local structure, structure B, shown in projection in Fig. 9. The corresponding atomic parameters are given in Table 5. Structure B also contains the structural units found in the average structure and, like structure A, has only fully occupied sites.

The principal difference between the two structures is that in structure A the Mo_6O_{18} cluster layers have a molybdenum sheet as a near neighbour on one side and

Table 4. *Selected interatomic distances (Å) for structure A ($P6_3mc$)*

S.u.'s are given in parentheses and are calculated from the s.u.'s in the atomic positions in the average structure.

La1—O1 × 2	2.4 (1)	Mo1—Mo1 × 2	2.675 (7)
La1—O2	2.75 (2)	Mo1—Mo4 × 2	2.678 (7)
La1—O3	3.16 (1)	Mo1—O7 × 2	1.977 (8)
La1—O7 × 2	3.30 (1)	Mo1—O8	2.05 (1)
La1—O8 × 2	2.39 (1)	Mo1—O9 × 2	2.041 (8)
La1—O9 × 2	2.903 (9)		
La1—O10	2.48 (2)	Mo2—Mo2 × 2	2.56 (2)
		Mo2—Mo3	2.87 (1)
La2—O1 × 6	2.76 (1)	Mo2—O1 × 2	1.99 (2)
La2—O4 × 3	2.78 (2)	Mo2—O2	2.06 (2)
La2—O9 × 3	3.09 (2)	Mo2—O4	2.09 (2)
		Mo2—O5 × 2	2.03 (2)
La3—O5 × 3	2.95 (3)		
La3—O7 × 6	2.804 (5)	Mo3—Mo3	2.65 (2)
La3—O8 × 3	2.42 (2)	Mo3—O1 × 2	2.07 (8)
		Mo3—O3	2.03 (1)
La4—O6 × 3	2.52 (4)	Mo3—O5	2.13 (3)
La4—O7 × 6	2.797 (5)	Mo3—O6 × 2	1.98 (1)
La4—O10 × 1	2.16 (3)		
		Mo4—Mo4 × 2	2.678 (7)
		Mo4—O4 × 2	2.041 (8)
		Mo4—O6	2.05 (1)
		Mo4—O6 × 2	1.977 (8)

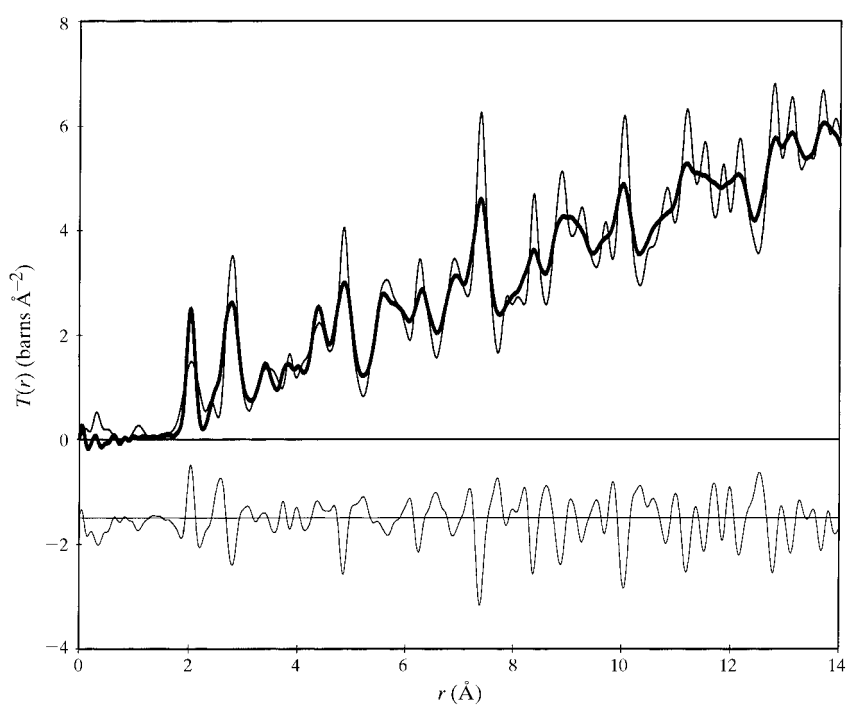

Fig. 7. $T(r)_{exp}$ (heavy line) and $T(r)$ calculated for $LaMo_2O_5$ from the Rietveld refinement in space group $P6_3/mmc$ structure (light line). The difference is shown below.

a layer of lanthanum oxide on the other, while in structure B there are two types of Mo_6O_{18} layers: half the Mo_6O_{18} layers in structure B have molybdenum sheets as near neighbours both above and below, and the other half have lanthanum oxide layers as near neighbours both above and below.

Total correlation functions $T(r)$ from 0–13.7 Å were generated from structures A and B and compared with $T(r)_{exp}$. Thermal broadening was introduced by:

(i) calculating $\sigma_{ll'}$ values for the partial correlation functions from the U values obtained in the Rietveld refinement of the structure of $LaMo_2O_5$ in space group $P6_3/mmc$ using the relationships given in equations (11) and (12); and

(ii) using $\sigma_{ll'}$ values for σ_{Mo-O}, σ_{Mo-Mo} and σ_{O-O} derived from U values obtained in the Rietveld refinement of the structure of $Zn_2Mo_3O_8$ and assuming $\sigma_{La-O} = \sigma_{Zn-O}$, $\sigma_{La-Mo} = \sigma_{Zn-Mo}$ and $\sigma_{La-La} = \sigma_{Zn-Zn}$.

The first method yielded a much better fit to $T(r)$ at short range than the average model [for structure A ($P6_3mc$) $R_{T(r)}$(1.5–3.3 Å) = 0.19 and $R_{T(r)}$(1.5–13.7 Å) = 0.125], but it was clear that these $\sigma_{ll'}$ values were too high. The second method gave much better agreement between theoretical and experimental $T(r)$ at both short and medium range [for structure A ($P6_3mc$) $R_{T(r)}$(1.5–3.3 Å) = 0.194 and $R_{T(r)}$(1.5–13.7 Å) = 0.091, and for structure B ($P\bar{3}m1$) $R_{T(r)}$(1.5–3.3 Å) = 0.194 and $R_{T(r)}$(1.5–13.7 Å) = 0.083], and $T(r)_{calc}$ and $T(r)_{exp}$ for the two models using these partial $\sigma_{ll'}$ values are compared in Fig. 10. Also shown in Fig. 10 is a comparison of $T(r)_{calc}$ for the two models. It is not surprising that the partial $\sigma_{ll'}$ values obtained from the Rietveld refinement of the structure of $LaMo_2O_5$ in $P6_3/mmc$ are in error, since U in these refinements will contain both a static and a thermal contribution. Partial $\sigma_{ll'}$ values derived from the Rietveld refinement of $Zn_2Mo_3O_8$ contain only a thermal contribution, since the structure is ordered, and we expect that these will provide good estimates of thermal-broadening parameters for use in modelling $LaMo_2O_5$ $T(r)$. The values used for σ_{Mo-O} and σ_{O-O} are most important, as can be seen in Fig. 11, which shows the weighted partial correlation functions $t_{ll'}$ after thermal broadening. For the final fit to $T(r)$, we adjusted σ_{O-O} and obtained the best fit with σ_{O-O} = 0.15 Å. Fig. 12 shows the variation of $R_{D(r)}$(1.5–3.3 Å) with σ_{O-O} for structure A. The final fit to $T(r)$ is shown in Fig. 13; the R values obtained [for

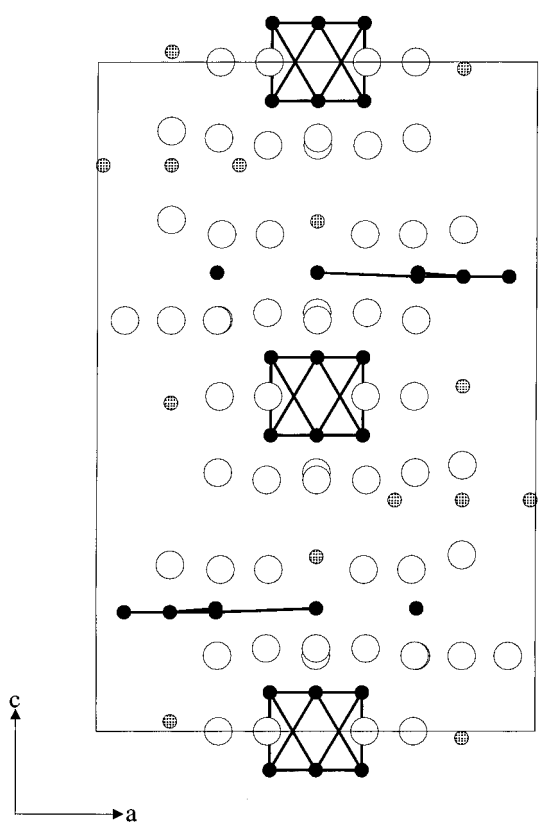

Fig. 8. Structural model for $LaMo_2O_5$ (structure A) in space group $P6_3mc$ projected down the [120] direction (solid circles: Mo; open circles: O; spotted circles: La). Only Mo—Mo bonds are shown. Light lines indicate the unit cell.

Table 5. *Atomic parameters for structure B (space group $P\bar{3}m1$) used to model T(r)*

	Multiplicity	x	y	z
La1	6	0.5112	0.4888	0.6562
La2	2	0	0	0.2400
La3	2	1/3	2/3	0.5160
La4	2	1/3	2/3	0.0120
Mo1	6	0.1066	0.8934	0.9428
Mo2	6	0.7690	0.2310	0.8132
Mo3	6	0.4390	0.5610	0.8220
Mo4	6	0.8934	0.1066	0.4428
O1	12	0.3300	0.0000	0.2420
O2	2	1/3	2/3	0.2650
O3	2	2/3	1/3	0.2480
O4	6	0.8862	0.772	0.6234
O5	6	0.4400	0.8800	0.1157
O6	6	0.5464	0.7732	0.8870
O7	6	0	0.3339	0
O8	6	0.4536	0.2268	0.3870
O9	6	0.8862	0.7724	0.8770
O10	2	1/3	2/3	0.3990
O11	6	0	0.3339	1/2

Derived $\sigma_{ll'}$'s for the partial correlation functions, and agreement factors $R_{T(r)}$ and $R_{D(r)}$ for the three modelling regimes: (i) from the Rietveld refinement for $LaMo_2O_5$ σ_{O-O} = 0.060, σ_{Mo-O} = 0.070, σ_{Mo-Mo} = 0.070, σ_{La-La} = 0.147, σ_{La-O} = 0.114, σ_{La-Mo} = 0.115 Å, $R_{T(r)}$(1.5–3.3 Å) = 0.190, $R_{T(r)}$(1.5–13.7 Å) = 0.132, $R_{D(r)}$(1.5–3.3 Å) = 0.326, $R_{D(r)}$(1.5–13.7 Å) = 0.631; (ii) from the $Zn_2Mo_3O_8$ Rietveld refinement σ_{O-O} = 0.095, σ_{Mo-O} = 0.087, σ_{Mo-Mo} = 0.080, σ_{La-La} = 0.088, σ_{La-O} = 0.092, σ_{La-Mo} = 0.084 Å, $R_{T(r)}$(1.5–3.3 Å) = 0.194, $R_{T(r)}$(1.5–13.7 Å) = 0.083, $R_{D(r)}$(1.5–3.3 Å) = 0.331, $R_{D(r)}$(1.5–13.7 Å) = 0.424; (iii) from the $Zn_2Mo_3O_8$ Rietveld refinement with σ_{O-O} fixed at 0.15 Å σ_{O-O} = 0.150, σ_{Mo-O} = 0.087, σ_{Mo-Mo} = 0.080, σ_{La-La} = 0.088, σ_{La-O} = 0.092, σ_{La-Mo} = 0.084 Å, $R_{T(r)}$(1.5–3.3 Å) = 0.108, $R_{T(r)}$(1.5–13.7 Å) = 0.063, $R_{D(r)}$(1.5–3.3 Å) = 0.184, $R_{D(r)}$(1.5–13.7 Å) = 0.320.

Table 6. *Motifs of mutual adjunction, coordination numbers (CN) and bond-order sums ($\sum s_i$) for structure A ($P6_3mc$)*

	O1	O2	O3	O4	O5	O6	O7	O8	O9	O10	CN	$\sum s_i$
Mo1							2/1	1/1	2/2		5	3.32
Mo2	2/1	1/3		1/1	2/2						6	3.81
Mo3	2/1		1/3		1/1	2/2					6	3.71
Mo4				2/2		1/1	2/1				5	3.32
La1	2/1	1/3	1/3				2/2	2/2	2/2	1/3	11	3.07
La2	6/1			3/1					3/1		12	2.14
La3					3/1		6/1	3/1			12	2.99
La4						3/1	6/1			1/1	10	3.29
CN	4	6	6	4	4	4	6	4	5	4		
$\sum s_i$	1.97	2.08	2.16	1.96	1.88	2.45	1.85	1.91	1.63	2.27		

structure A ($P6_3mc$) $R_{T(r)}$(1.5–3.3 Å) = 0.108 and $R_{T(r)}$(1.5–13.7 Å) = 0.063, and for structure B ($P\bar{3}m1$) $R_{T(r)}$(1.5–3.3 Å) = 0.108 and $R_{T(r)}$(1.5–13.7 Å) = 0.063] are almost as good as those obtained for $Zn_2Mo_3O_8$. However, it must be noted that we have included in this final model some allowance for static disorder as well as thermal disorder in the oxygen positions by adjusting σ_{O-O}.

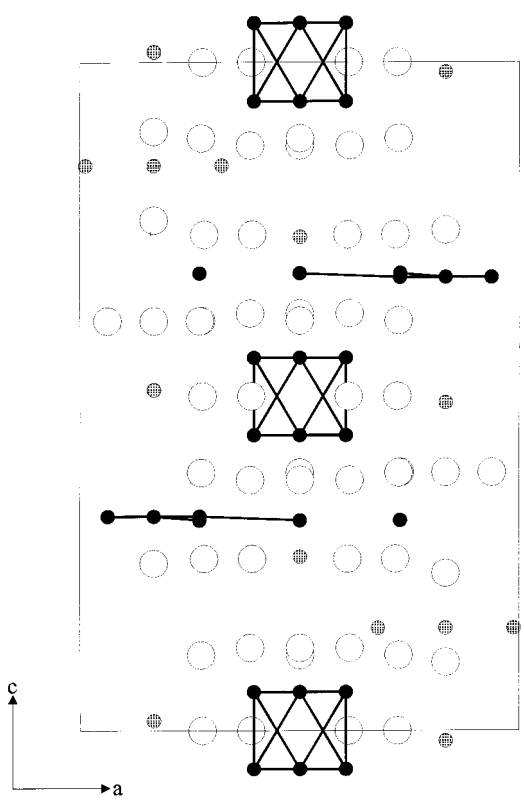

Fig. 9. Structural model for $LaMo_2O_5$ (structure B) in space group $P\bar{3}m1$ projected down the [120] direction (solid circles: Mo; open circles: O; spotted circles: La). Only Mo—Mo bonds are shown. Light lines indicate the unit cell.

6. Discussion

Both structure A ($P6_3mc$) and structure B ($P\bar{3}m1$) produce a good fit to $T(r)_{exp}$ over the r range 1.5–13.7 Å. The fit to $T(r)$ at short distances, r = 1.5–3.3 Å, is excellent for both structures [structure A ($P6_3mc$) $R_{T(r)}$(1.5–3.3 Å) = 0.108, structure B ($P\bar{3}m1$) $R_{T(r)}$(1.5–3.3 Å) = 0.108 *cf.* $Zn_2Mo_3O_8$ $R_{T(r)}$(1.5–3.3 Å) = 0.101], showing that our models describe the local structure well. The short-range structure and connectivity are nearly identical in the two models. This can be seen from the motifs of mutual adjunction (Hoppe, 1980) given in Table 6 (structure A, $P6_3mc$) and Table 7 (structure B, $P\bar{3}m1$). Comparison of these tables shows that the only change in the nearest-neighbour coordination is that O(7) in structure A is replaced by O(7) and O(11) in structure B. The two O atoms have different coordination polyhedra, but on average the same coordination as structure A ($P6_3mc$). The bond-order sums show how the local bonding requirements of molybdenum and oxygen are fulfilled in both structure A and structure B. Only beyond 3.30 Å (see Fig. 13) do differences occur between the two models. Tables 6 and 7 also contain bond-length–bond-order calculations for the two structures (Brown & Wu, 1976). Molybdenum–oxygen bond orders (s_{Mo-O}) for a molybdenum-to-oxygen bond of length R were calculated using $s_{Mo-O} = (R/R_1)^{-6}$ with R_1 = 1.882 Å (for a bond order of 1), and lanthanum–oxygen bond orders (s_{La-O}) for a lanthanum–oxygen bond of length R were calculated using $s_{La-O} = (R/R_1)^{-6.5}$ with R_1 = 2.167 Å (for a bond order of 1). We prefer to use the expression and parameters from Brown & Wu (1976) rather than Brown & Altermatt (1985) because we have found these to be reliable in previous work on molybdenum in lower oxidation states (Hibble & Fawcett, 1995). Further confirmation of their appropriateness is that they yield an average oxidation state for molybdenum of 3.54, extremely close to the value expected from the chemical formula $La^{III}(Mo^{3.5})_2(O^{-II})_5$. This can be compared with an average oxidation state for molybdenum of 3.99 in

Table 7. *Motifs of mutual adjunction, coordination numbers (CN) and bond order sums ($\sum s_i$) in structure B ($P\bar{3}m1$)*

	O1	O2	O3	O4	O5	O6	O7	O8	O9	O10	O11	CN	$\sum s_i$
Mo1				2/2		1/1	2/2					5	3.32
Mo2	2/1	1/3		1/1	2/2							6	3.81
Mo3	2/1		1/3		1/1	2/2						6	3.71
Mo4								1/1	2/2		2/2	5	3.32
La1	2/1	1/3	1/3					2/2	2/2	1/3	2/2	11	3.07
La2	6/1			3/1					3/1			12	2.14
La3								3/1		1/1	6/2	10	3.29
La4					3/1	3/1	6/2					12	2.99
CN	4	6	6	4	4	4	4	4	5	4	6		
$\sum s_i$	1.97	2.08	2.16	1.96	1.88	2.45	1.79	1.91	1.63	2.27	2.37		

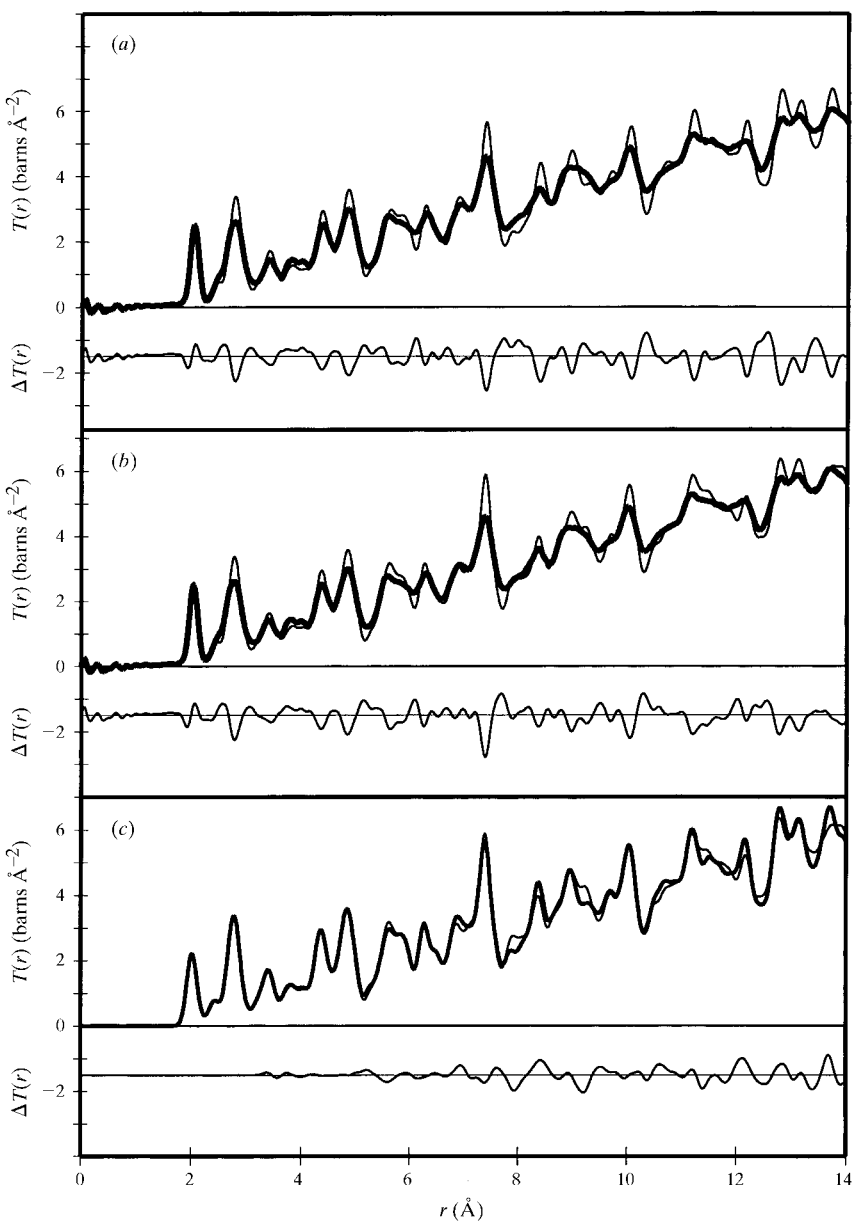

Fig. 10. (*a*) $T(r)_{exp}$ (heavy line), $T(r)$ calculated for $LaMo_2O_5$ $P6_3mc$ structure (light line) and difference (below); (*b*) $T(r)_{exp}$ (heavy line), $T(r)$ calculated for $LaMo_2O_5$ $P\bar{3}m1$ structure (light line) and difference (below); (*c*) $T(r)$ calculated for $LaMo_2O_5$ $P6_3mc$ structure (heavy line), $T(r)$ calculated for $LaMo_2O_5$ $P\bar{3}m1$ structure (light line) and difference (below) (using σ's obtained from $Zn_2Mo_3O_8$).

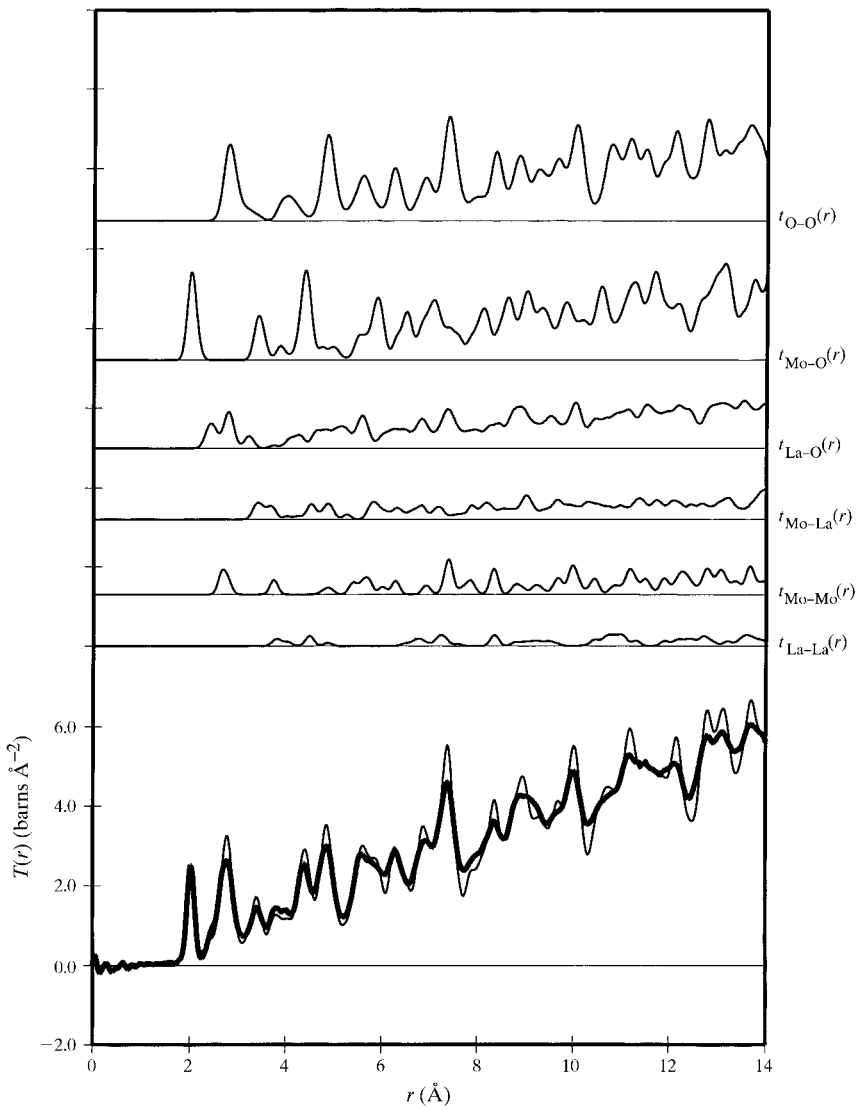

Fig. 11. Below: $T(r)_{exp}$ (heavy line) and $T(r)$ calculated for the $LaMo_2O_5$ $P6_3mc$ structure (light line). Above: contributions from the partials $t_{ll'}(r)$.

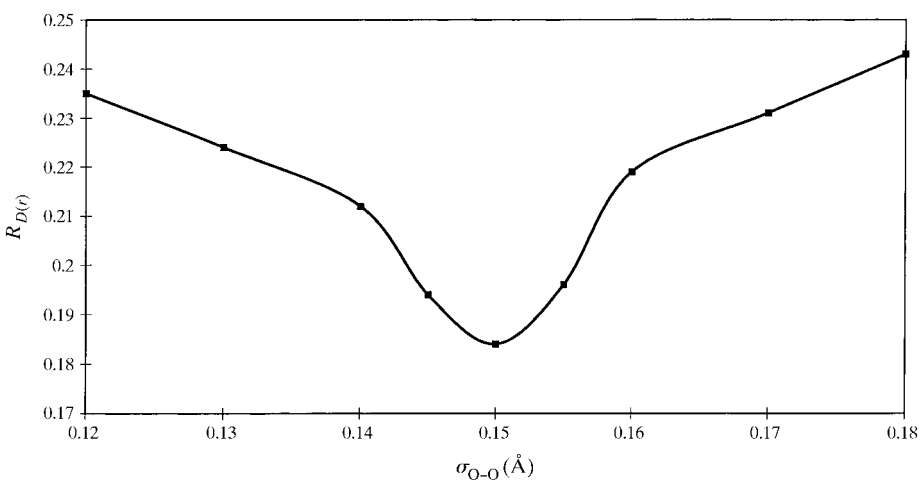

Fig. 12. Variation of $R_{D(r)}$(1.5–3.3 Å) with σ_{O-O} for $LaMo_2O_5$ (structure A), with the other σ values fixed at the values in Table 3 regime (ii).

$LaMo_2O_5$ calculated using the parameters of Brown & Altermatt (1985).

It is difficult to use $T(r)$ comparisons between the model and the experimental values over the r range 1.5–14 Å to differentiate between the validity of the two models [structure A ($P6_3mc$) $R_{T(r)}$(1.5–13.7 Å) = 0.0627, structure B ($P\bar{3}m1$) $R_{T(r)}$(1.5–13.7 Å) = 0.0630]. However, consideration of the Bragg-scattering intensities allows us to determine that structure A ($P6_3mc$) makes the major contribution to the average structure. Refining only the scale factors in Rietveld refinements gives R_{wp} = 0.065 for structure A ($P6_3mc$) and R_{wp} = 0.099 for structure B ($P\bar{3}m1$).

The identical short-range structure in structures A and B means that intergrowths of the two structures might be expected to occur easily. Elements of structure B with either two adjacent Mo layers or two adjacent La layers can also be produced by twinning of the $P6_3mc$ structure by addition of an inversion centre at the centre of the Mo_6O_{18} octahedron. Again, the identical short-range order of the two structures means this can occur with only minor perturbations of the local structure. This explains why disorder can easily arise in $LaMo_2O_5$ and how the average structure in $P6_3/mmc$ is produced.

An obvious possibility arising from this intergrowth model is that the additional weak broad Bragg peaks in

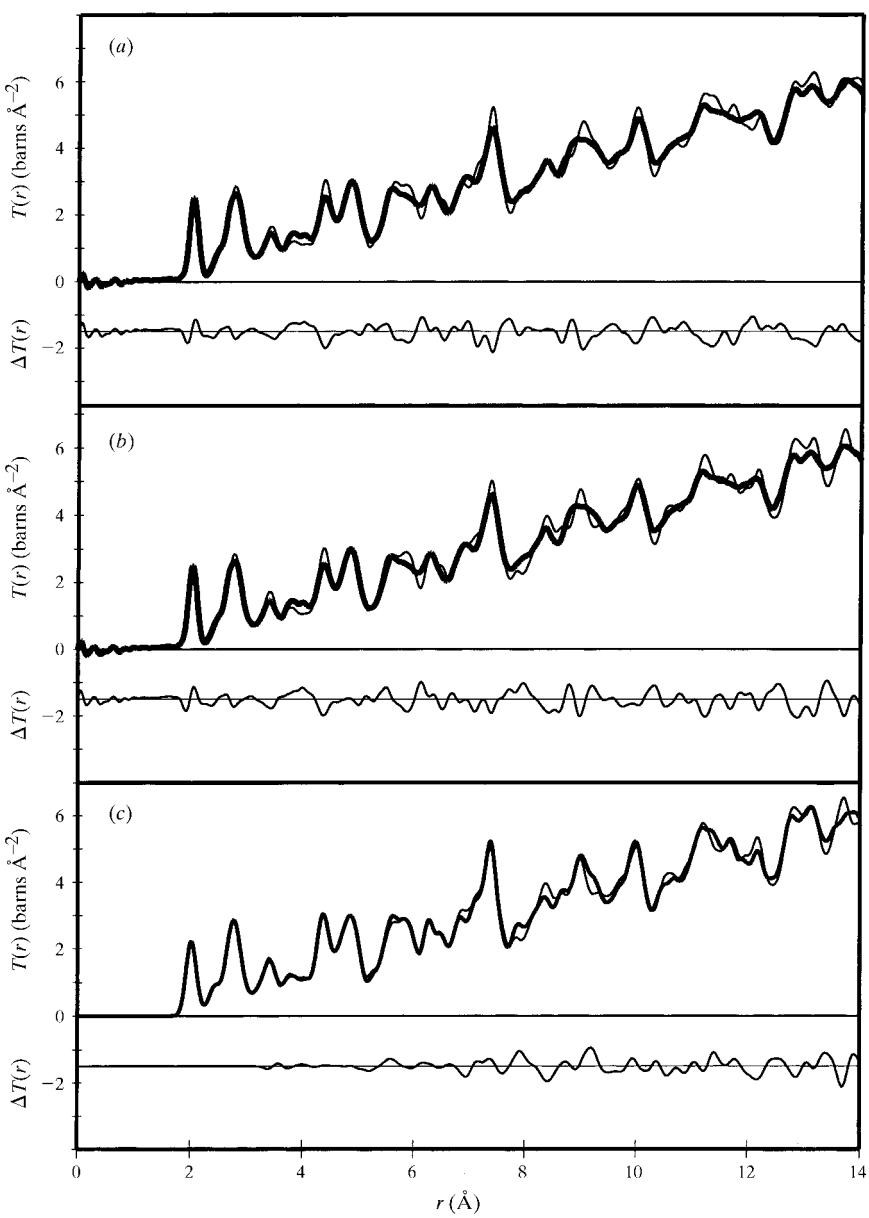

Fig. 13. Final fit to $T(r)$ using σ_{O-O} = 0.15. (*a*) $T(r)_{exp}$ (heavy line), $T(r)$ calculated for $LaMo_2O_5$ $P6_3mc$ structure (light line) and difference (below); (*b*) $T(r)_{exp}$ (heavy line), $T(r)$ calculated for $LaMo_2O_5$ $P\bar{3}m1$ structure (light line) and difference (below); (*c*) $T(r)$ (heavy line) calculated for $LaMo_2O_5$ $P6_3mc$, $T(r)$ calculated for $LaMo_2O_5$ $P\bar{3}m1$ structure (light line) and difference (below).

the diffraction pattern of $LaMo_2O_5$, which were unaccounted for in our Rietveld model, might arise from ordered intergrowths of structures A and B. To our surprise, we found that the additional peaks can be accounted for not by taking a multiple of the *c* axis but by doubling *a* and *b*. This larger cell with $a' = 2a$, $b' = 2b$ and $c' = c$ accounted for nearly all the remaining structure seen in the $(I_{obs} - I_{calc})$/s.u. plot. We plan a detailed high-resolution electron microscopy study to shed further light on how the two structures intergrow and a study of the electronic structure to give an insight into possible reasons for the doubling of *a* and *b*. These topics lie beyond the scope of the present work, which was to determine models for the local structure in $LaMo_2O_5$. One advantage of total neutron scattering studies is that the additional Bragg scattering not included in our Rietveld modelling is included in our calculation of $T(r)$. We can be confident that our local structures are correct and that major changes to the basic building blocks will not be needed in further modelling of Bragg scattering.

Although the fits to $T(r)_{exp}$ we obtain for our two models of the local structure in $LaMo_2O_5$ are good, neither structure A nor B gives as good a fit to $T(r)$ over the range r = 1.5–14 Å as we obtain in modelling the ordered structure $Zn_2Mo_3O_8$. Remaining discrepancies are probably owing to local static displacements where the structures intergrow, which we have not modelled. Some element of disorder has been subsumed in our final model, in which a standard deviation for the O–O partial correlation function higher than that expected for just a thermal contribution has been used. Another area in which our model may be deficient is in describing the La-atom positions and coordination. Inspection of Tables 6 and 7 shows that the bond-order sum around La2 is too low. It is possible that the La atoms are displaced from these ideal positions in the real structure. What does appear to be very well described in these models is the basic framework and Mo—O bond lengths, which yield valuable information on the structure and bonding in $LaMo_2O_5$.

7. Concluding remarks

We have succeeded in producing good models for the local structure of $LaMo_2O_5$ and have shown their validity by comparison of calculated $T(r)$'s with $T(r)$ determined from total neutron scattering studies. These local models contain the information on structural units that is the goal of the chemical crystallographer. We have shown how these local structures can be derived from the average structure, which fits the Bragg scattering, by removal of symmetry elements, and that the local structures are described in subgroups of the space group used to describe the average structure.

This work shows that total neutron scattering is extremely useful in the structure determination of disordered crystalline materials. By modelling the Bragg scattering the average structure is obtained. Modelling $T(r)$ obtained from total scattering gives information on local structure. Combining the two gives a much more complete structural picture than that obtained only from Bragg scattering. As always in structural studies of disordered materials, this study is not definitive and provides only a step along the way to a more complete structural description. We hope in future work to be able to explain the reason for the doubling of the *a* and *b* unit-cell parameters and to describe more accurately the disorder along *c*.

We thank the EPSRC for the provision of neutron diffraction facilities and a studentship for SPC, and the Royal Society for a Visiting Fellowship for SP.

References

Ansell, G. B. & Katz, L. (1966). *Acta Cryst.* **21**, 482–485.
Brown, I. D. & Altermatt, D. (1985). *Acta Cryst.* B**41**, 244–247.
Brown, I. D. & Wu, K. K. (1976). *Acta Cryst.* B**32**, 1957–1959.
David, W. I. F., Ibberson, R. M. & Matthewman, J. C. (1992). Report RAL-92-032. Rutherford Appleton Laboratory, Didcot, England.
David, W. I. F., Johnson, M. W., Knowles, K. J., Moreton-Smith, C. M., Crosbie, G. D., Campbell, E. P., Graham, S. P. & Lyall, J. S. (1986). Report RAL-86-102. Rutherford Appleton Laboratory, Didcot, England.
Dove, M. T., Keen, D., Hannon, A. C. & Swainson, I. P. (1997). *Phys. Chem. Mineral.* **24**, 311–317.
Hannon, A. C. (1993). Report RAL-93-063. Rutherford Appleton Laboratory, Didcot, England.
Hannon, A. C., Howells, W. S. & Soper, A. K. (1990). *Proceedings of the Second Workshop on Neutron Scattering Data Analysis (WONSDA2)*, edited by M. W. Johnson, IOP Conf. Ser. **107**, 193–211.
Hibble, S. J., Cooper, S. P., Hannon, A. C., Patat, S. & McCarroll, W. H. (1998). *Inorg. Chem.* **37**, 6839–6846.
Hibble, S. J. & Fawcett, I. D. (1995). *Inorg. Chem.* **34**, 500–508.
Hibble, S. J., Fawcett, I. D. & Hannon, A. C. (1997*a*). *Acta Cryst.* B**53**, 604–612.
Hibble, S. J., Fawcett, I. D. & Hannon, A. C. (1997*b*). *Inorg. Chem.* **36**, 1749–1753.
Hoppe, R. (1980). *Angew. Chem. Int. Ed. Engl.* **19**, 110–125.
Howells, W. S. (1980). Report RAL-80-017. Rutherford Appleton Laboratory, Didcot, England.
Koester, L. & Yelon, W. B. (1982). *Summary of Low Energy Neutron Scattering Lengths and Cross Sections.* Netherland Research Foundation, Department of Physics, Petten, The Netherlands.
Lorch, E. (1969). *J. Phys. C*, **2**, 229–237.
Louca, D., Egami, T., Brousha, E. L., Roder, H. & Bishop, A. R. (1997). *Phys. Rev. B*, **56**, 8475–8478.
Soper, A. K., David, W. I. F., Sivia, D. S., Dennis, T. J. S., Hare, J. P. & Prassides, K. (1992). *J. Phys. Condens. Matter*, **4**, 6087–6094.

Soper, A. K., Howells, W. S. & Hannon, A. C. (1989). Report RAL-89-046. Rutherford Appleton Laboratory, Didcot, England.

Teslic, S., Egami, T. & Viehland, D. J. (1997). *Phys. Chem. Solids*, **57**, 1537–1543.

Toby, B. H. & Egami, T. (1992). *Acta Cryst.* A**48**, 336–346.